Quantum metrology with molecular ensembles

Marcus Schaffry,[1] Erik M. Gauger,[1] John J. L. Morton,[2] Joseph Fitzsimons,[1,3] Simon C. Benjamin,[1,4] and Brendon W. Lovett[1,5]

[1]*Department of Materials, University of Oxford, Parks Road, Oxford OX1 3PH, United Kingdom*

[2]*CAESR, The Clarendon Laboratory, Department of Physics, University of Oxford, OX1 3PU, United Kingdom*

[3]*Institute for Quantum Computing, University of Waterloo, Waterloo, Ontario, Canada*

[4]*Centre for Quantum Technologies, National University of Singapore, 3 Science Drive 2, Singapore 117543*

[5]*School of Engineering and Physical Sciences, Heriot-Watt University, Edinburgh EH14 4AS, United Kingdom*

(Received 14 July 2010; published 28 October 2010)

The field of quantum metrology promises measurement devices that are fundamentally superior to conventional technologies. Specifically, when quantum entanglement is harnessed, the precision achieved is supposed to scale more favorably with the resources employed, such as system size and time required. Here, we consider measurement of magnetic-field strength using an ensemble of spin-active molecules. We identify a third essential resource: the change in ensemble polarization (entropy increase) during the metrology experiment. We find that performance depends crucially on the form of decoherence present; for a plausible dephasing model, we describe a quantum strategy, which can indeed beat the standard strategy.

DOI: 10.1103/PhysRevA.82.042114 PACS number(s): 03.65.Ta, 03.65.Ud, 03.65.Yz, 07.55.Ge

I. INTRODUCTION

Quantum metrology deals with the physical limits to measurement. Typically, one prepares a probe system of size K in a suitable initial state; this system acquires information about the quantity of interest, and then the probe system is measured. The process may be repeated either with a series of probes over time or, as in the present analysis, with multiple probe systems simultaneously. The way in which the probe is prepared is closely related to the uncertainty of the parameter estimation: if prepared in a nonentangled state, then the minimal uncertainty achievable scales with $1/\sqrt{K}$ [1], the so-called standard quantum limit (SQL). However, this limit can be beaten if we allow arbitrary states for the preparation of the probe system (i.e., if we include entangled states), as demonstrated in recent experiments [2–5]. In idealized cases, the minimal uncertainty achievable scales with $1/K$—the Heisenberg limit [6]—which can be achieved by making use of special entangled states such as Greenberger-Horne-Zeilinger (GHZ) states or maximally path-entangled $\frac{1}{\sqrt{2}}(|N,0\rangle + |0,N\rangle)$ (NOON) states [7].

In optical quantum metrology, the probe system is a particular state of K photons, for example, a NOON state, which is a superposition of all K photons in channel A with all photons in channel B. When an optical element inducing an unknown phase shift is placed in channel A, then the probe acquires an internal phase K times as great as that which would be acquired by a single photon, and information about this phase is measured through an interference effect. In the present analysis, we consider an analogous experiment involving K atomic spins in a large molecule, which probes the strength of an external magnetic field. An essential difference is that we consider a large ensemble of probe molecules, which are necessarily prepared, exposed to the field, and ultimately measured *collectively* [8,9]—that is, addressing of individual probe molecules is impossible.

The dynamics of an ensemble is typically observed by measuring the free-induction decay (FID) spin signal. Monitoring the FID can be seen as a continuous and simultaneous measurement of two noncommuting observables [10]. Here, the observed system is barely altered by the measurement, as the number of spins in a typical sample is usually so large. This type of measurement has not yet been analyzed in the context of quantum metrology. Rather, recent studies have looked at the effect of temperature on the Fisher information of three types of states [11] and wave-form estimation and its implications for quantum sensing [12].

II. MAGNETIC FIELD SENSING

In this paper, we compare two strategies for measuring a small shift δB of a probe magnetic field from a reference field in a spin ensemble setting [8,9]. This problem is equivalent to measuring the Larmor frequency $\delta = \frac{\delta B}{\gamma}$ of a precessing spin in the probe field, where γ is the gyromagnetic ratio. In the *quantum* strategy, we consider a macroscopic ensemble of N sensor molecules each consisting of K spins, where each molecule is prepared in a very sensitive entangled state (see Fig. 1). This state senses the field for a wait time T_w by acquiring a phase $K\,\delta T_w$. We then map the phase onto one spin of the molecule from which it can be read out by observing the FID. As a performance benchmark, we compare this to the *classical* or *standard* strategy, where we determine the Larmor frequency by observing the FID of the same number of uncoupled spins. We will focus on the resources consumed by the two strategies and on the impact of decoherence.

The role of decoherence is very nontrivial. In the absence of decoherence and for a perfect projective measurement, the lowest achievable uncertainty in estimating δ scales with $1/K\sqrt{N}$ for the quantum strategy and $1/\sqrt{KN}$ for the classical strategy [6]. Hence, the discrepancy in the precision of the two strategies increases with the size of the entangled state K. However, the spins will be subject to decoherence in any real-world experiment, and the sensitive entangled states will decohere faster than separable states when K becomes larger [13,14]. This increased effective decoherence rate competes with the enhanced precision, making it difficult to predict the performance of the quantum strategy.

In the following, we will determine lower bounds for the uncertainty of the parameter estimation from a measured FID for both strategies. First, we must generate a suitable entangled state to obtain enhanced sensitivity with the quantum strategy,

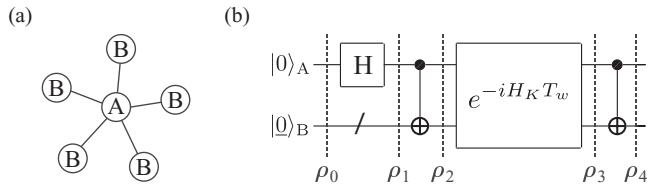

FIG. 1. (a) Schematic of a sensor molecule with five satellites. (b) Quantum circuit employed in the quantum strategy.

meaning we require some amount of quantum control over the molecules. The details of how this is accomplished are unimportant, and we will, in the following, consider the example shown in Fig. 1; molecules with this star topology have been employed in recent experiments [8,9]. Each molecule consists of one central spin A and $K-1$ noninteracting satellites of type B. The satellites interact with the central spin through an Ising-type interaction, leading to the following Hamiltonian in an external magnetic field [in natural units (i.e., $\hbar = 1$)]:

$$H_K = \gamma\,\delta\sigma_z^A + \delta\sum_{j=1}^{K-1}\sigma_z^{B_j} + J\sum_{j=1}^{K-1}\sigma_z^A\otimes\sigma_z^{B_j}, \qquad (1)$$

where σ_z denotes the usual Pauli matrix with eigenvalues $\pm\frac{1}{2}$. δ denotes the Zeeman splitting of the B spins, and $\gamma = \frac{\gamma_A}{\gamma_B}$ denotes the ratio of the gyromagnetic numbers of A and B, and we assume $\gamma \approx 1$. J describes the Ising interaction strength and is only necessary for implementing the multiqubit gates in the quantum strategy, not for the sensing process. δ is the parameter to be estimated.

We focus on the fundamental comparison between classical and quantum strategies given a fully polarized initial state of the sample:

$$\rho_0 = |0\rangle_A\langle 0|_A \otimes |0\cdots 0\rangle_B\langle 0\cdots 0|_B = |0\underline{0}\rangle\langle 0\underline{0}|, \qquad (2)$$

where the underscore denotes the state of the $K-1$ satellite spin register. For the example molecule shown, the entangled state can be constructed from this initial state by applying the pulse sequence shown in Fig. 1 [i.e., first a Hadamard gate on the central spin and then a controlled-NOT (CNOT) gate (control qubit = central spin, target qubits = satellites)]. The resulting GHZ state $\frac{1}{\sqrt{2}}(|0\underline{0}\rangle + |1\underline{1}\rangle)$ freely evolves for a time T_w, acquiring phase K times faster than a single spin.[1] However, at the same time, it is also more vulnerable to decoherence. In practice, the dephasing rate of an individual spin $\alpha = -\frac{1}{T_2^*} < 0$ is limited by inhomogeneous broadening [15], thus, we can neglect spin-flip processes. Of course, the dephasing rate of the GHZ state $\beta < 0$ is related to α, and we will discuss this dependence later. The state of the system, after the wait time T_w, is then

$$\rho_3 = \tfrac{1}{2}(|0\underline{0}\rangle\langle 0\underline{0}| + |1\underline{1}\rangle\langle 1\underline{1}| + e^{-K\,\delta T_w\, i+\beta T_w}|0\underline{0}\rangle\langle 1\underline{1}| + e^{K\,\delta T_w\, i+\beta T_w}|1\underline{1}\rangle\langle 0\underline{0}|). \qquad (3)$$

[1]Strictly, this is only a GHZ state for $K > 2$ and a Bell state for $K = 2$. In Ref. [8], this state is referred to as a NOON state because it describes a superposition of N spins up and N spins down.

To measure the acquired phase $K\,\delta T_w$, we map the GHZ state onto the central spins by applying a CNOT gate. These spins are then measured by observing the decay of the transverse magnetization at $M \in \mathbb{N}$ discrete points in time, separated by the sampling time t_s. The observed signal x_m at time mt_s ($m = 0,\ldots,M-1$) can be modeled as a sum of Gaussian distributed noise b_m and the ideal signal $\hat{x}_m = \langle X + iY\rangle(mt_s)$ [16],

$$x_m = \hat{x}_m + b_m = ce^{K\,\delta T_w\, i+\beta T_w}e^{\delta m\, t_s+\alpha m t_s} + b_m, \qquad (4)$$

where c is a proportionality factor that depends on the number of molecules in the sample. A simulation of the FID is shown in Fig. 2.

A suitable metric for the precision of the measurement is the Cramér-Rao bound (CRB) b^{CR} [16], which essentially offers a lower bound on the uncertainty (standard deviation) σ_{p_ℓ} of an estimated parameter p_ℓ ($\ell = 1,\ldots,P$):

$$\sigma_{p_\ell} \geqslant b_{p_\ell}^{\mathrm{CR}} = \sqrt{(F^{-1})_{\ell\ell}}. \qquad (5)$$

Here, F denotes the Fisher information [17] given by the real part of a complex-valued matrix product,

$$F = \frac{1}{\sigma^2}\,\mathrm{Re}\,(D^\dagger D), \qquad (6)$$

where $D_{ij} = \frac{\partial\hat{x}_i}{\partial p_j}$, and the partial derivatives are evaluated at the parameters that we are going to estimate. In our case, the parameters are c, α, and δ. $\sigma = \sigma_r = \sigma_i$ denotes the standard deviation of the real (imaginary) part of the noise. Inverting the 3×3 Fisher information matrix, we obtain

$$b_{\delta,\mathrm{GHZ}}^{\mathrm{CR}} = \frac{e^{-\beta T_w}}{\sqrt{\sum_{m=0}^{M-1}(KT_w + mt_s)^2\exp(2\alpha m t_s)}}\frac{\sigma}{c}. \qquad (7)$$

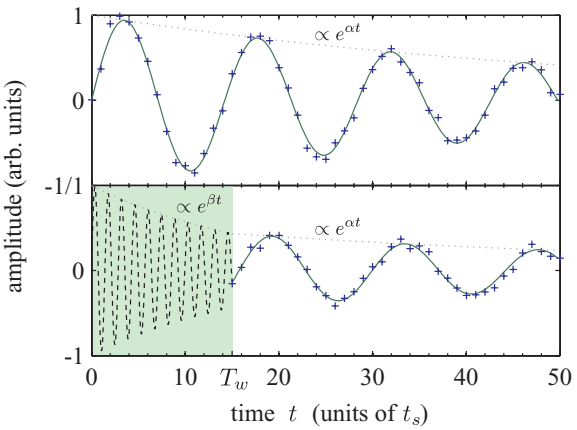

FIG. 2. (Color online) Simulation of the FID of the classical (upper) and quantum strategy (lower); see Eqs. (4) and (9). The simulated measurement points (crosses) were chosen randomly from a Gaussian distribution with a standard deviation of 0.05. In the classical strategy, we observe uncoupled precessing spins, and the strength of the probe field is given by the oscillation frequency. In the quantum strategy, a GHZ state senses the field for a time T_w without producing a signal but acquiring phase K times faster than a single spin and dephasing at a rate β. The acquired phase is mapped onto the central spin, and the FID is measured. The strength of the magnetic field can now be estimated from the phase and the oscillation frequency.

Next, we determine the CRB for the classical strategy. Here, we are given NK identical and uncoupled spins. We obtain the relevant signal by rotating the initial state ρ_0 into the xy plane with a global Hadamard gate followed by measuring the transverse magnetization. The resulting density matrix evolves as

$$\rho(t) = \frac{1}{2}\begin{pmatrix} 1 & e^{i\,\delta t+\alpha t} \\ e^{-i\,\delta t+\alpha t} & 1 \end{pmatrix} \tag{8}$$

giving rise to a measured signal of the following form:

$$x'_m = c' e^{\delta m\, t_s i+\alpha m t_s} + b'_m. \tag{9}$$

Analogously, to Eq. (7) we obtain the CRB for this signal:

$$b^{\mathrm{CR}}_{\delta,\mathrm{STD}} = \frac{1}{\sqrt{\sum_{m=0}^{M'-1}(mt_s)^2\,\exp\left(2\alpha m t_s\right)}}\frac{\sigma'}{c'}. \tag{10}$$

This expression is a lower bound on the uncertainty for independent spins against which we will benchmark the quantum strategy. As the signal-to-noise ratio (SNR) $\frac{c'}{\sigma'}$ scales with the square root of the number of spins in the sample, we get the same scaling behavior as for the SQL. For a high SNR achieved by a sufficiently large number of molecules N, there exists an efficient estimator, which matches the accuracy predicted by the CRB [18]. Hence, we can directly use Eqs. (7) and (10) to compare the two strategies.

III. OBSERVATION OF THE FULL FID

First, we need to specify a fair comparison with the same resource allocation for both strategies. For conventional quantum metrology with projective measurements, the challenging question of a fair resource comparison has recently been addressed in Ref. [19]. In the present case of ensemble quantum metrology, we will, at first, allow both strategies to observe the full FID while consuming the von Neumann entropy of $1N$ spins. As we have defined it, the quantum strategy consumes one spin per molecule (the central spin A) in the measurement, and all other spins remain pure. This implies that we must also only measure N spins instead of KN spins for the classical strategy, meaning that the SNR of both measurements is equal $\frac{c'}{\sigma'} = \frac{c}{\sigma}$.

At first sight, this way of counting resources may look biased toward the quantum case, as we do not seem to take the satellite spins into account. Nonetheless, our comparison is fair: The $K-1$ satellite spins act as an antenna to pick up phase more rapidly, yet they are not consumed (this is a direct consequence of the dephasing model of decoherence). After the quantum strategy is complete, the central spin is measured (its polarization is lost), but all satellite spins are back in the pure state $|\underline{0}\rangle$ and could be recycled to obtain a further parameter estimate. The accuracy of such an estimate, made using any sensible protocol on these remaining $(K-1)N$ spins, can be no worse than that obtained using the standard strategy. This observation validates the classical resource count stated in the previous paragraph.

The ratio of Eqs. (7) and (10) can be approximated by an integral expression [assuming the sampling rate resolves the decay (i.e., $t_s \ll T_2^*$)]:

$$R_\infty := \frac{b^{\mathrm{CR}}_{\delta,\mathrm{STD}}}{b^{\mathrm{CR}}_{\delta,\mathrm{GHZ}}} \approx \sqrt{\frac{\int_0^\infty (KT_w+t)^2\,\exp\left(2\alpha t\right)\,dt}{e^{-2\beta T_w}\int_0^\infty t^2\,\exp\left(2\alpha t\right)dt}} \tag{11}$$

$$= e^{\beta T_w}\sqrt{1-2K\alpha T_w(1-K\alpha T_w)}. \tag{12}$$

Whenever $R_\infty > 1$, the quantum strategy outperforms the classical strategy with respect to the precision of the parameter estimation.

We have not yet specified how the dephasing rate β of the GHZ state relates to the dephasing rate α of a single spin, and now, we will discuss a number of different decoherence models for the GHZ state.

First, we consider $\beta = \alpha$, implying that the GHZ state does not decohere faster than a single spin; this is expected for a given macroscopic magnetic-field inhomogeneity. In this case, there is, for any $K > 1$, a wait time T_w, for which the quantum strategy surpasses the classical one. Conversely, completely correlated or collective noise over each molecule has the most aggressive effect on the GHZ state [20]. Here, the noise can be described with a single Lindblad operator $\sum_{j=1}^{K}\sigma_z$ and $\beta = K^2\alpha$, while, for uncorrelated noise, $\beta = K\alpha$ [21]. In general, we consider a power-law dependence of β on α (i.e., $\beta = K^p\alpha$, where $0 \leqslant p \leqslant 2$). In recent experiments, the decoherence rates for highly correlated solid-state spin states were obtained experimentally [22], revealing $p \approx 1/2$. The authors attributed this to non-Markovian correlated noise. A significantly smaller value for p was found in Ref. [9], where the T_2^* time of a single spin was determined to be 0.37 s and that of a 13-particle GHZ state was determined to be 0.28 s, which can be interpreted as a factor of $p \approx 0.11$.

The performance of the quantum sensor depends critically on the value of p. One can easily check that, for $1 \leqslant p \leqslant 2$, $R_\infty < 1$ for any $T_w > 0$, and $R_\infty = 1$ only for $T_w = 0$. Therefore, we conclude that the precision of the quantum method never outperforms the precision of the standard method, if $1 \leqslant p \leqslant 2$. In contrast, for $p < 1$, there is an optimal nonzero, K-dependent, wait time T_w for which $R_\infty > 1$. Specifically, calculating the optimal waiting time T_w that

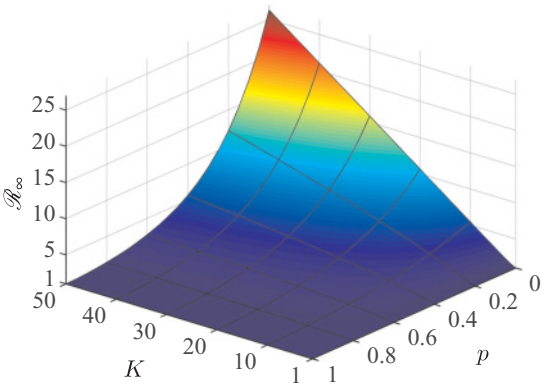

FIG. 3. (Color online) The maximal $\mathscr{R}_\infty$ for a given K as a function of K and p. $\mathscr{R}_\infty > 1$ implies that the quantum strategy outperforms the standard strategy.

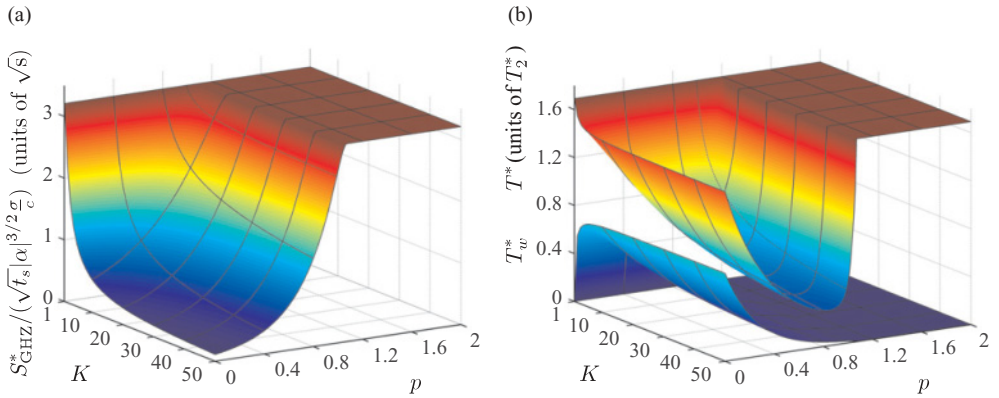

FIG. 4. (Color online) (a) Minimal (optimized over T and T_w) uncertainty of the parameter estimation for the quantum strategy per $\sqrt{\mathrm{Hz}}$ [i.e., $S^*_{\mathrm{GHZ}}/(\sqrt{t_s}|\alpha|^{3/2}\frac{\sigma}{c})$ in dependence of K and p]. (b) The corresponding optimal times T^* (upper surface) and T_w^* (lower surface) as units of T_2^* for which the minimum in (a) is attained in dependence of K and p.

gives rise to a maximum of $\mathscr{R}_\infty$ (for a given K and $p < 1$) yields

$$\mathscr{R}_\infty = \max_{T_w} \mathscr{R}_\infty = \frac{K^{1/2-p}\sqrt{K+\sqrt{K^2-K^{2p}}}}{\exp\left[\frac{1}{2}(1-K^{p-1}+\sqrt{1-K^{2p-2}})\right]}, \tag{13}$$

which scales like $\frac{\sqrt{2}}{e}K^{1-p}$ to leading order (see Fig. 3). Therefore, the standard strategy can indeed be beaten with a quantum strategy if the decoherence of the GHZ state is not too aggressive (i.e., for $p < 1$). Moreover, we see that, under this condition, the precision of the estimation improves monotonically as K increases. As a special case, we consider $p = 0$, here, $\mathscr{R}_\infty$ increases linearly in K; this means that the uncertainty of the parameter estimation with the optimized quantum strategy scales as $1/K$, analogous to the Heisenberg limit.

IV. RESTRICTED PROCESS TIME

So far, we have neglected time as a resource, focusing instead on system size and the consumption of initial polarization (maximizing the von Neumann entropy of one spin per molecule). It is interesting to extend our analysis to a restricted process time, meaning only a part of the FID can be observed. Since the first part of the FID contains most information, this would enable a better sensor by a series of repeated runs in a given time window T_{tot} if one had the ability to reset the spins to their initial state after time T, for example, with an optical switch. We assume that this can be done instantly, and then, the uncertainty of the parameter estimation of this series is given by

$$\frac{1}{\sqrt{T_{\mathrm{tot}}/T}} b^{\mathrm{CR}}_{\delta,\mathrm{STD}} =: \frac{1}{\sqrt{T_{\mathrm{tot}}}} S_{\mathrm{STD}} \tag{14}$$

and analogously for $b^{\mathrm{CR}}_{\delta,\mathrm{GHZ}}$ and S_{GHZ}. Obviously, one would choose the length of a time slice T optimally [i.e., in such a way that the uncertainty per $\sqrt{\mathrm{Hz}}$ (i.e., S_{STD} and S_{GHZ} are minimal)]. For the classical strategy, we find by using the integral approximation for the CRB from before and the numerical optimization that

$$S^*_{\mathrm{STD}} := \min_T S_{\mathrm{STD}} = \kappa\sqrt{t_s}|\alpha|^{3/2}\frac{\sigma'}{c'}, \tag{15}$$

with $\kappa \approx 3.21\sqrt{\mathrm{s}}$, which is attained for the optimal time $T^* \approx 1.69T_2^*$. In the quantum strategy, S_{GHZ} also depends on T_w, the amount of time for which the spins are in the GHZ state. In contrast to the classical strategy, here, the minimum depends on the system parameters K and p. We have not been able to find an analytic expression for $S^*_{\mathrm{GHZ}} := \min_{T,T_w} S_{\mathrm{GHZ}}$; and, we therefore performed a numerical optimization with the results displayed in Fig. 4. As in our first comparison, we assume that the SNR for both strategies is equal. If aggressive noise is affecting the GHZ state, the optimal quantum strategy is basically the optimal standard strategy, as $T^* \to 1.69T_2^*$ and $T_w^* \to 0$, when $p \to 2$. For small p and large K, however, the quantum strategy significantly outperforms the standard strategy. Interestingly, the quantum strategy can now beat the optimized standard strategy for values p that are slightly larger than 1.

V. CONCLUSION

In conclusion, we have presented a framework for analyzing the performance of quantum metrology using spin ensembles. This framework incorporates the special nature of the nonprojective measurement process, and leads one to consider the polarization change during the protocol as a kind of resource consumption. We find that the decoherence model plays a defining role in this framework, and we have identified the parameter regime where a certain quantum strategy can beat the standard classical strategy.

ACKNOWLEDGMENTS

We thank Y. Matsuzaki and S. Simmons for discussions. This work was supported by the EPSRC through QIP IRC (Grants No. GR/S82176/01 and No. GR/S15808/01), the National Research Foundation and Ministry of Education, Singapore, the DAAD, and the Royal Society.

[1] L. Pezzé and A. Smerzi, Phys. Rev. Lett. **102**, 100401 (2009).
[2] D. Leibfried *et al.*, Nature (London) **438**, 639 (2005).
[3] T. Nagata *et al.*, Science **316**, 726 (2007).
[4] L. Pezzé and A. Smerzi, Phys. Rev. Lett. **100**, 073601 (2008).
[5] I. Afek, O. Ambar, and Y. Silberberg, Science **328**, 879 (2010).
[6] V. Giovannetti, S. Lloyd, and L. Maccone, Science **306**, 1330 (2004); Phys. Rev. Lett. **96**, 010401 (2006).
[7] H. Lee, P. Kok, and J. P. Dowling, J. Mod. Opt. **49**, 2325 (2002).
[8] J. A. Jones *et al.*, Science **324**, 1166 (2009).
[9] S. Simmons, J. A. Jones, S. D. Karlen, A. Ardavan, and J. J. L. Morton, Phys. Rev. A **82**, 022330 (2010).
[10] *Quantum Entanglement and Information Processing: Lecture Notes of the Les Houches Summer School 2003 (Les Houches)*, edited by D. Estève, J.-M. Raimond, and J. Dalibard (Elsevier Science & Technology, 2004).
[11] K. Modi, M. Williamson, H. Cable, and V. Vedral, e-print arXiv:1003.1174 [quant-ph].
[12] M. Tsang and C. M. Caves, e-print arXiv:1006.5407 [quant-ph].
[13] A. Shaji and C. M. Caves, Phys. Rev. A **76**, 032111 (2007).
[14] S. F. Huelga, C. Macchiavello, T. Pellizzari, A. K. Ekert, M. B. Plenio, and J. I. Cirac, Phys. Rev. Lett. **79**, 3865 (1997).
[15] M. H. Levitt, *Spin Dynamics: Basics of Nuclear Magnetic Resonance* (Wiley, West Sussex, 2002).
[16] S. Cavassila *et al.*, J. Magn. Reson. **143**, 311 (2000).
[17] A. van den Bos, *Handbook of Measurement Science* (Wiley, New York, 1982).
[18] Y. Bresler and A. Macovski, IEEE Trans. Acoust., Speech, Signal Process. **34**, 1081 (1986).
[19] M. Zwierz, C. A. Pérez-Delgado, and P. Kok, e-print arXiv:1004.3944 [quant-ph] (accepted by Phys. Rev. Lett.).
[20] A. Shimizu and T. Miyadera, Phys. Rev. Lett. **89**, 270403 (2002); G. M. Palma, K.-A. Suominen, and A. K. Ekert, Proc. R. Soc. London, Ser. A **452**, 567 (1996).
[21] L. Aolita, R. Chaves, D. Cavalcanti, A. Acín, and L. Davidovich, Phys. Rev. Lett. **100**, 080501 (2008).
[22] H. G. Krojanski and D. Suter, Phys. Rev. Lett. **93**, 090501 (2004); **97**, 150503 (2006).